NOON state of Bose atoms in the double-well potential via an excited-state quantum phase transition

A. A. Bychek,[1,2] D. N. Maksimov,[1,3] and A. R. Kolovsky[1,2]

[1]*Kirensky Institute of Physics, Federal Research Center KSC SB RAS, 660036 Krasnoyarsk, Russia*

[2]*Siberian Federal University, 660041 Krasnoyarsk, Russia*

[3]*Reshetnev Siberian State University of Science and Technology, 660037 Krasnoyarsk, Russia*

(Received 1 February 2018; published 28 June 2018)

We suggest a simple scheme for creating a NOON state of repulsively interacting Bose atoms in the double-well potential. The protocol consists of two steps. First, by setting atom-atom interactions to zero, the system is driven to the upper excited state. Second, the interactions are slowly increased and, simultaneously, the interwell tunneling is decreased to zero. We analyze fidelity of the final state to the NOON state depending on the number of atoms, ramp rate, and fluctuations of the system parameters. It is shown that for a given fidelity the ramp rate scales algebraically with the number of atoms.

DOI: 10.1103/PhysRevA.97.063624

I. INTRODUCTION

Nonclassical states of bosonic ensembles play important roles in quantum computing, measurement, and communication [1–3]. Among many different implementations [4–10] the two-mode Bose-Hubbard model [11–36] is the most popular playground thanks to its versatility, relative simplicity, and experimental accessibility with ultracold atoms in optical potentials [2,18,23,26,34,35]. In this paper we propose a recipe for generating NOON states [37], also known as large cat sates [12], in the two-site Bose-Hubbard model. It should be mentioned from the very beginning that, due to decoherence processes inevitably present in a laboratory experiment (particle losses, fluctuations of the optical potential, etc.), the NOON state can be obtained only for a relatively small number of atoms. In other words, in the thermodynamic limit $N \to \infty$ one always gets a statistical mixture of two states with all atoms localized in either of two wells—the phenomenon known as spontaneous localization or parity-symmetry-breaking phase transition. One of the goals of this paper is to estimate the maximal number of atoms for which one can create the NOON state with the present day experimental facilities.

Formally, the NOON state is the ground state of the one-dimensional *attractive* Bose-Hubbard model [13,17,20] in the strong interaction regime. In practice, however, this state is hard to reach because the NOON state is fragile to particle losses caused by the collision instability [38]. To avoid this problem we consider *repulsive* atom-atom interactions where the NOON state appears to be the upper energy state of the system. In what follows we show that this state can be reached in the course of adiabatic passage through an excited-state quantum phase transition (ESQPT) [39–41]. It is generally believed that such an adiabatic passage would require extremely long evolution time, which scales exponentially with the number of particles [21]. Here, by detailed examination of the system spectrum in a view of the Landau-Zener tunneling, we demonstrate that the evolution time actually scales *algebraically* with the number of bosons N. A pseudoclassical interpretation of the adiabatic passage with the ESQPT corresponding to a separatrix crossing in the classical phase space is provided.

II. SYSTEM OVERVIEW

We consider $N \gg 1$ Bose atoms with repulsive interactions in the double-well potential. This system is known to be well described by the two-site Bose-Hubbard Hamiltonian [13,14],

$$\widehat{H} = -\frac{J}{2}(\hat{a}_2^\dagger \hat{a}_1 + \hat{a}_2 \hat{a}_1^\dagger) + \frac{U}{2}\sum_{l=1,2} \hat{n}_l(\hat{n}_l - 1) + \delta(\hat{n}_2 - \hat{n}_1), \tag{1}$$

where J is the hopping matrix element, U is the microscopic interaction constant, $\hat{a}_l$ and $\hat{a}_l^\dagger$ are the bosonic annihilation and creation operators, $\hat{n}_l$ is the number operator, and δ is the difference between the on-site energies. For N bosons the Hilbert space of the Hamiltonian (1) of dimension $\mathcal{N} = N + 1$ is spanned by Fock states,

$$|N_1, N_2\rangle = |N/2 - n, N/2 + n\rangle \equiv |n\rangle, \quad |n| \leqslant N/2, \tag{2}$$

where $N_1 + N_2 = N$. Above we used a symmetric parametrization to label the Fock states by a single quantum number n (N is assumed to be even). The full spectrum of the system is shown in Fig. 1 where we introduced the macroscopic interaction constant $g = UN/2$ and set the hopping matrix element to $J = 1 - g$. Thus, the case of $g = 0$ corresponds to the system of noninteracting bosons whereas in the case of $g = 1$ the interwell tunneling is completely suppressed. It is easy to prove that the spectrum is equidistant for $g = 0$ and quadratic for $g = 1$ with all energy levels except the ground state being twofold degenerate [22]. The spectrum for intermediate g possesses the quantum separatrix and can be understood by employing the pseudoclassical approach which we review in Sec. III.

Among the eigenstates $|\Psi_j\rangle$ of the Hamiltonian (1) of particular interest are the states with minimal and maximal energies. For $g = 0$ the ground state of the system is a Bose-Einstein condensate with all particles occupying the symmetric

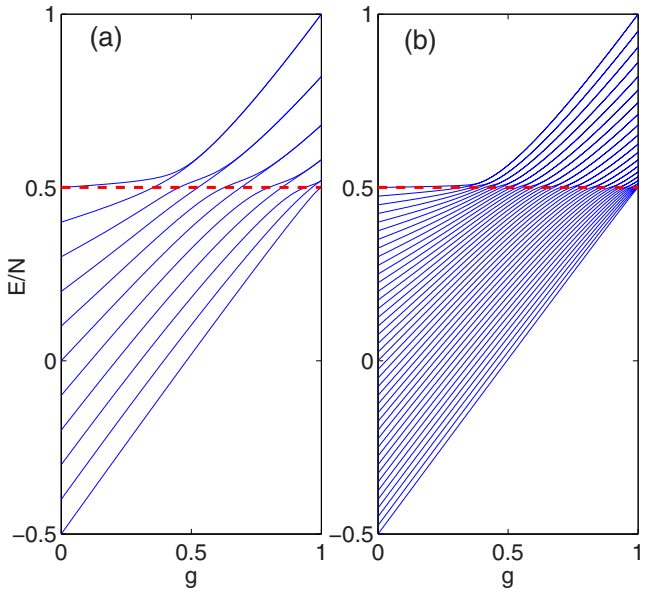

FIG. 1. Energy spectrum of $N = 10$ (left) and $N = 40$ (right) bosons against the macroscopic interaction constant $g = UN/2$. (The other parameters are $J = 1 - g$ and $\delta = 0$.) The quantum separatrix is marked by the red dashed line.

single-particle state,

$$|\Psi_0(g=0)\rangle = \frac{1}{\sqrt{2^N N!}}(a_1^\dagger + a_2^\dagger)^N|\text{vac}\rangle, \tag{3}$$

whereas the upper energy state is a Bose-Einstein condensate with all particles occupying the antisymmetric single-particle state,

$$|\Psi_N(g=0)\rangle = \frac{1}{\sqrt{2^N N!}}(a_1^\dagger - a_2^\dagger)^N|\text{vac}\rangle. \tag{4}$$

Let us follow these states under variation of g. At each value of g eigenfunctions are found as an expansion over the Fock states (2),

$$|\Psi_j(g)\rangle = \sum_{n=-N/2}^{N/2} c_n^{(j)}(g)|n\rangle, \tag{5}$$

For $j = 0$ and $j = N$ the results are shown in Fig. 2. It is seen that the ground state transforms into the fragmented condensate [22],

$$|\Psi_0(g=1)\rangle = |N/2, N/2\rangle, \tag{6}$$

whereas the upper energy state evolves into the NOON state,

$$|\Psi_N(g=1)\rangle = |\text{NOON}\rangle \equiv \frac{1}{\sqrt{2}}(|N,0\rangle + |0,N\rangle). \tag{7}$$

Next we consider the time evolution of the system according to the Schrödinger equation,

$$i\frac{d}{dt}|\psi\rangle = \widehat{H}(g)|\psi\rangle, \quad J = 1 - g, \tag{8}$$

with the interaction constant g growing linearly from 0 to 1 during the time-interval $T = 1/\nu$. In Fig. 3(a) we present the results of numerical simulations of the system dynamics for $|\psi(t=0)\rangle = |\Psi_N(g=0)\rangle$ and $\nu = 0.1$. Shown are squared

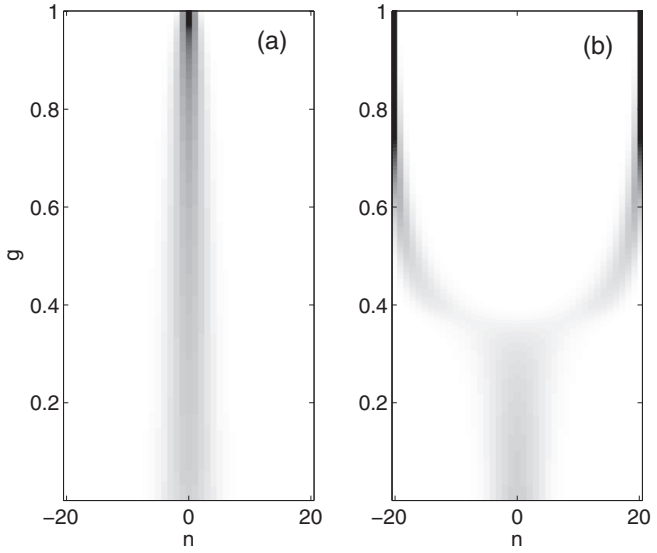

FIG. 2. Squared absolute values of expansion coefficients Eq. (5) of the ground (left) and upper energy (right) states against the macroscopic interaction constant g.

absolute values of the expansion coefficients $c_n(t) = \langle n|\psi(t)\rangle$. One can see in Fig. 3(b) that the final state $|\psi(t=T)\rangle$ does not ideally coincide with the target NOON state Eq. (7). With a smaller ramp rate, however, the result is almost perfect, see Fig. 3(c). In the next sections we analyze the discussed adiabatic passage in more detail and quantify the final state $|\psi(t=T)\rangle$. To pay credit to other works we mention that adiabatic passage for the ground state of the attractive Bose-Hubbard model was considered earlier in Refs. [20,42] and a different adiabatic passage, which involves the rising potential barrier which separates a Bose-Einstein condensate into two parts, was analyzed in Refs. [14,15,19,24].

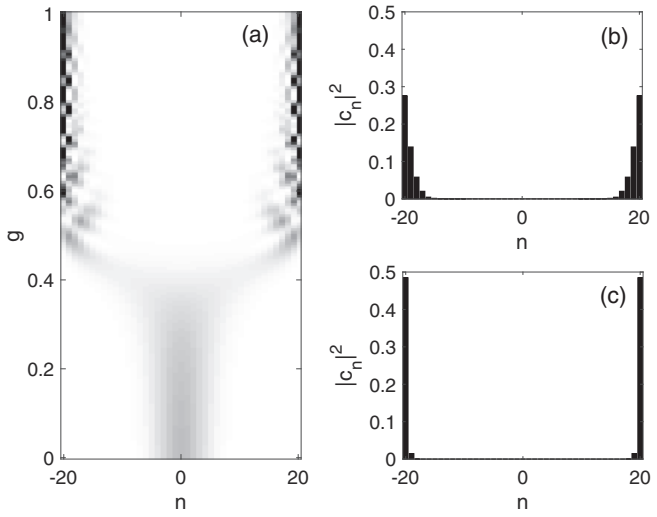

FIG. 3. Panel (a): Squared absolute values of expansion coefficients over the Fock basis as the function of $g = \nu t$ for the adiabatic passage with $\nu = 0.1$. Panels (b) and (c) compare the final states of the system for $\nu = 0.1$ and $\nu = 0.025$.

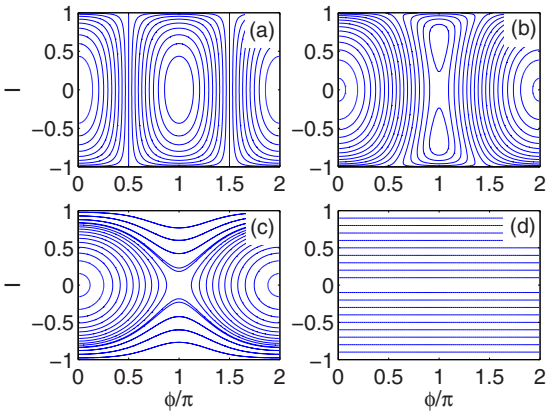

FIG. 4. Phase portraits of the classical Hamiltonian (9) for (a) $g = 0$, (b) $g = 0.4$, (c) $g = 0.7$, and (d) $g = 1$.

III. PSEUDOCLASSICAL APPROACH

To get a deeper insight into the discussed adiabatic passage we resort to the pseudoclassical approach. This approach borrows its ideas from the semiclassical method in single-particle quantum mechanics to address the spectral and dynamical properties of the system of N interacting bosons with $1/N$ playing the role of Planck's constant [43–46]. Formally, the creation and annihilation operators are substituted with C-numbers as $\hat{a}_l/\sqrt{N} \to a_l$ and $\hat{a}_l^\dagger/\sqrt{N} \to a_l^*$, which also implies rescaling of the Hamiltonian as $\widehat{H}/N \to H$. For the two-site Bose-Hubbard model this leads to the classical Hamiltonian [11],

$$H = \frac{g}{2} I^2 - \frac{J}{2}\sqrt{1 - I^2}\cos\,\phi, \quad J = 1 - g, \tag{9}$$

where $g = UN/2$ is the macroscopic interaction constant.

Figure 4 shows the phase portrait of the system (9) at four different values of g: 0, 0.4, 0.7, and 1. By using the relation $I = \sin\,\theta$ phase portraits of the system can be also drawn on a sphere of the unit radius. In this representation the line $I = 1$ ($I = -1$) reduces to a single point—the north (south) pole of the sphere. For $g = 0$ the phase portrait contains two elliptic points at $(I,\phi) = (0,0)$ (minimal energy) and $(I,\phi) = (0,\pi)$ (maximal energy), see Fig. 4(a). As g is increased above $g_{cr} = 1/3$ the latter elliptic point bifurcates into two elliptic points at $(I,\phi) = (\pm I^*,\pi)$, where I^* is a function of g. With a further increase in g the island around the point $(I,\phi) = (0,0)$ vanishes whereas the islands around $(I,\phi) = (\pm I^*,\pi)$ monotonically grow, finally leading to the phase-space portrait shown in Fig. 4(d).

The depicted phase portraits suffice to find the energy spectrum shown in Fig. 1 by using the semiclassical quantization rule where the phase volume encircled by a trajectory is required to be a multiple of the effective Planck constant $h = 1/N$. Then the central island around the point $(I,\phi) = (0,0)$ gives energy levels below the quantum separatrix whereas two symmetric islands around $(I,\phi) = (\pm I^*,\pi)$ give degenerate levels above the quantum separatrix. The details are given in Ref. [45] where it was demonstrated that the pseudoclassical approach provides an accurate approximation to the exact spectrum even for $N = 10$.

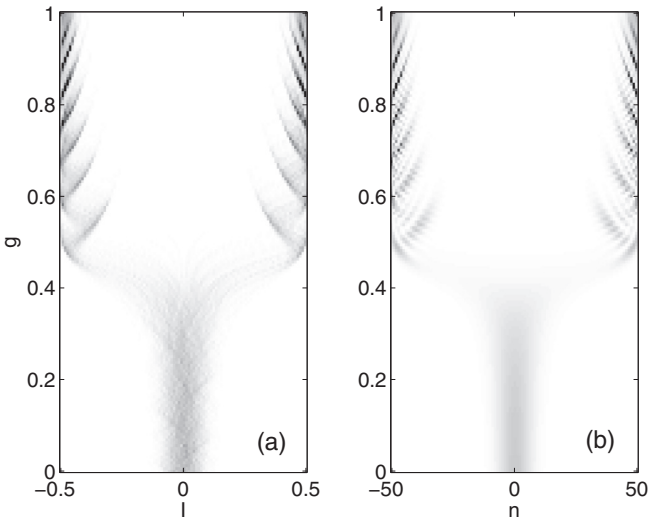

FIG. 5. Comparison between the classical (left panel) and the quantum (right panel) dynamics. Parameters are $\delta = 0$, $\nu = 0.1$, and $N = 100$.

Let us now study the dynamics of the classical system (9) when both g and J vary in time as $g = \nu t$ and $J = 1 - g$. As the initial condition we take an ensemble of particles with the probability distribution given by the two-dimensional Gaussian centered at the elliptic point $(I,\phi) = (0,\pi)$. For comparison with quantum dynamics the width of the Gaussian is adjusted to $\sigma = \sqrt{N}$. The left panel in Fig. 5 shows the evolution of the classical distribution function $\rho(I,t)$ for $N = 100$. (We stress one more time that the latter parameter determines only the width of the initial distribution.) The left panel in Fig. 5 should be compared with the right panel showing the quantum evolution. The observed agreement underlines the classical phenomenon behind the quantum results discussed in the previous section. Classically, the particles are captured into the upper and lower islands emerging after bifurcation of the elliptic point $(I,\phi) = (0,\pi)$ and then transported towards $I = 1$ and $I = -1$, respectively. The phenomenon of capturing into (and releasing from) an elliptic island was considered earlier in Ref. [47] in a different context. It involves the crossing of an instantaneous separatrix that, in turn, was analyzed in Ref. [48].

To conclude this section we discuss the effect of nonzero δ. For $\delta \neq 0$ the emerging islands have different sizes, which makes $\rho(I,t)$ asymmetric with respect to $I \to -I$. To characterize this asymmetry we introduce the population imbalance,

$$G = \int_0^1 \rho(I,T)dI - \int_{-1}^0 \rho(I,T)dI. \tag{10}$$

If δ is increased the population imbalance (10) grows monotonically, approaching $|G| = 1$, see Fig. 6. Importantly, the imbalance also grows if ν is decreased, and for any finite δ the imbalance is unity in the limit $\nu \to 0$.

IV. LANDAU-ZENER TUNNELING AND FIDELITY TO THE NOON STATE

In the previous section we explained the quantum results depicted in Fig. 2 by using the pseudoclassical approach. The

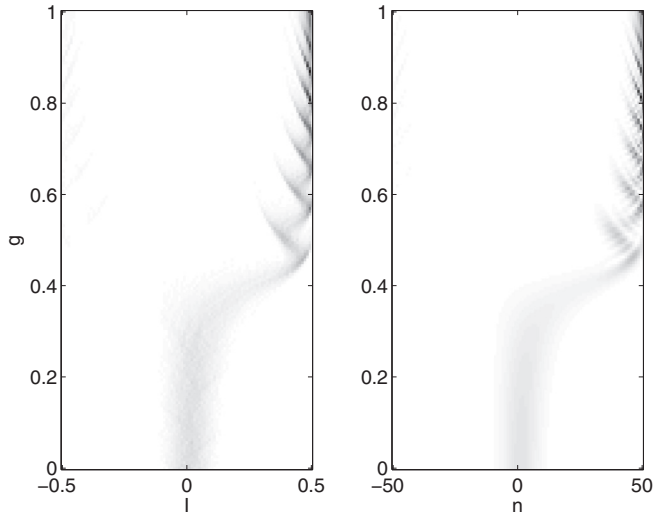

FIG. 6. The same as in Fig. 5 with $\delta = 0.01$.

quantum-mechanical explanation of these results is based on the notion of Landau-Zener tunneling. Due to this phenomenon several energy levels become populated as we follow the upper most level in Fig. 1 with a finite sweeping rate. This is illustrated in Fig. 7(a) which shows the populations of the instantaneous energy levels $P_j(t)$,

$$P_j(t) = |\langle \Psi_j(g = \nu t)|\psi(t)\rangle|^2 \tag{11}$$

for $\nu = 0.1$ and $N = 30$. Note that only even levels are populated because of different symmetries of eigenstates of the Hamiltonian (1) with odd and even indices j. To quantify the effect of Landau-Zener tunneling we introduce the fidelity,

$$F = |\langle \mathrm{NOON}|\psi(T)\rangle|^2, \tag{12}$$

which characterizes how close the final state is to the target NOON state. In the limit $\nu \to 0$ it is enough to take into account only the nearest high-energy level of the same (even)

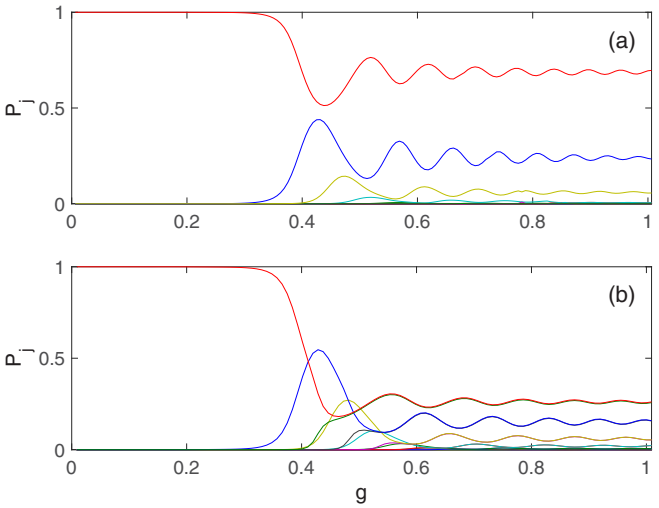

FIG. 7. Populations of the instantaneous energy levels for $N = 30$, $\nu = 0.1$, and $\delta = 0$ (upper panel) and $\delta = 0.0001$ (lower panel).

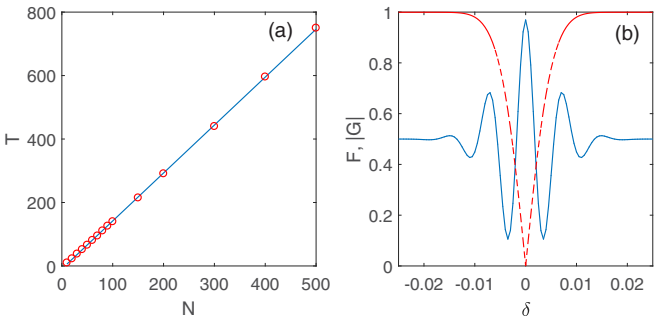

FIG. 8. Left panel: Minimal evolution time T ensuring fidelity $F = 0.99$ versus the number of bosons N. Right panel: Population imbalance $|G|$ (dashed line) and fidelity F (solid line) as the function of δ for $N = 40$ and $\nu = 0.025$.

symmetry, which alone determines fidelity of the final state through the celebrated Landau-Zener equation,

$$F = 1 - \exp\left(-\frac{\pi\Delta^2}{2|\alpha|\nu}\right). \tag{13}$$

In Eq. (13) Δ is the energy gap between the uppermost level and the next level of the same symmetry, $\nu = 1/T$ is the sweeping rate, and α is determined by the angle at which two levels approach each other. Since the energy gap Δ and $|\alpha|$ scale algebraically with $1/N$, we expect that the evolution time T has to be increased proportionally to the number of particles to ensure a given fidelity. Direct numerical simulations of the adiabatic passage for different N's confirm this hypothesis, see Fig. 8(a). It is interesting to discuss the depicted result with respect to the recent laboratory experiment [34] which studies the parity-symmetry-breaking phase transition for $N \approx 4500$ attractively interacting atoms in a double-well potential. Taking $J/h = 40$ Hz and the evolution time of $\sim$1 s we get $N \approx 30$, and this number can be easily increased by relaxing the fidelity to $F = 0.9$ and using a time-dependent sweeping rate of $\nu = \nu(t)$ that optimizes the adiabatic passage. We stress that the above estimate is obtained under the assumption of negligible decoherence processes which we will discuss in Sec. V.

Next we analyze the effect of nonzero $\delta \ll J$ in the Hamiltonian (1) from the quantum-mechanical viewpoint. Nonzero δ breaks the reflection symmetry of the system so that eigenstates of the Hamiltonian (1) at $g \gg J$ are given by the Fock states $|N/2 - n, N/2 + n\rangle$ and $|N/2 + n, N/2 - n\rangle$ but not their symmetric or antisymmetric superpositions. (In particular, $|\Psi_N\rangle \approx |N, 0\rangle$ and $|\Psi_{N-1}\rangle \approx |0, N\rangle$.) This drastically changes Fig. 7(a)—now both odd and even instantaneous energy levels become populated during the adiabatic passage, see Fig. 7(b). For the considered extremely small value of δ this difference simply reflects a change in the basis and, physically, both Figs. 7(a) and 7(b) describe the same process, which results in the NOON state as the final state of the system. However, for a larger δ we see considerable deviation from the NOON state, see Fig. 8(b). In particular, in full analogy with the classical result, the population imbalance $|G|$ approaches the unity if $|\delta|$ is increased.

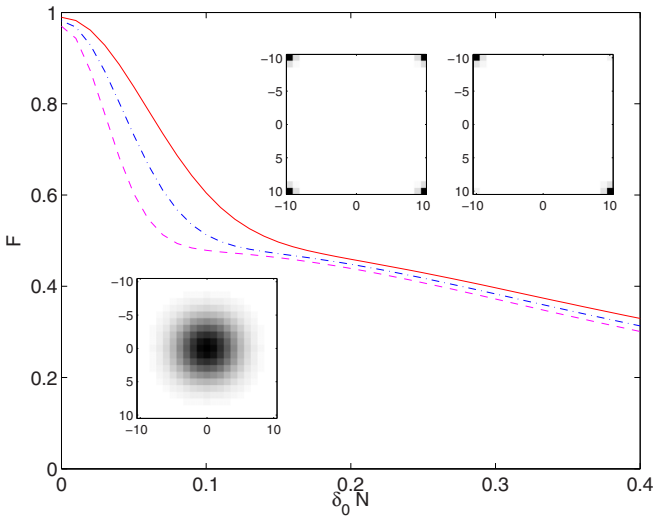

FIG. 9. Fidelity (14) as the function of the noise amplitude for $N = 10$ and $\nu = 0.1$ (solid line), $N = 20$ and $\nu = 0.05$ (dashed-dotted line), and $N = 40$ and $\nu = 0.025$ (dashed line). The insets show the initial density matrix for $N = 20$ (lower-left corner) and final density matrices for $\delta_0 = 0$ and $\delta_0 = 0.1/N$ (upper-right corner).

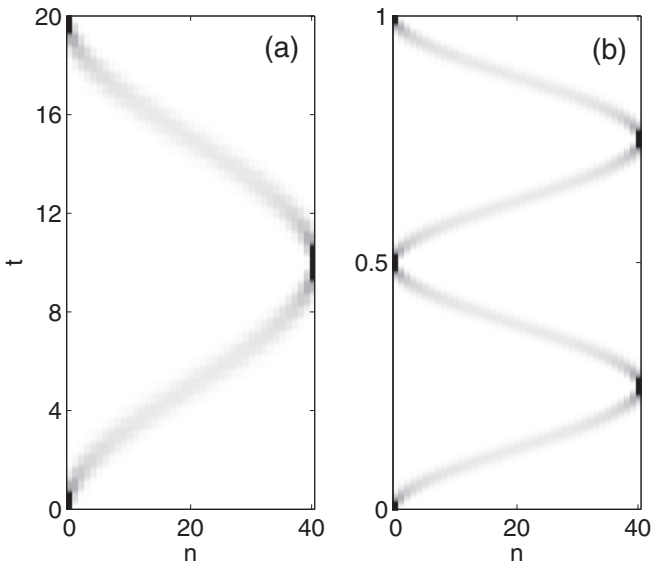

FIG. 10. Populations of eigenstates of the Hamiltonian (1) as the function of time. [Note that for $g = 0$ the eigenstates of (1) are given by $|N-n,n\rangle$ where n now denotes the number of particles in the antisymmetric single-particle state.] Parameters are $N = 40$, $g = 0$, $J = 1$, $\omega = J$, $\delta_0 = 0.05$ (left panel), and $N = 40$, $g = 0$, $J = 0.01$, $\delta = 1$ (right panel).

V. DECOHERENCE EFFECTS

The result depicted in Fig. 8(a) proves that, at least in principle, one can create an arbitrary large cat state by simply increasing the duration of the adiabatic passage proportionally to the number of particles N. This, however, implicitly assumes the absence of any decoherence process [21] and precision control over the system parameters, in the first place, over parameter δ. In this section we discuss decoherence caused by fluctuations of δ, which are unavoidable in a laboratory experiment.

In the presence of fluctuations the fidelity (12) should be redefined as

$$F = \langle \mathrm{NOON}|\mathcal{R}(T)|\mathrm{NOON}\rangle, \quad \mathcal{R}(t) = \overline{|\psi(t)\rangle\langle\psi(t)|}, \qquad (14)$$

where the bar denotes the average over fluctuations. To be specific, we assume that $\delta(t)$ is the white noise with a vanishing mean value, i.e., $\overline{\delta(t)\delta(t')} = \delta_0^2\delta(t-t')$. Then the density matrix $\mathcal{R}(t)$ is easy to show to obey the following master equation [49]:

$$\frac{d\mathcal{R}}{dt} = -i[\widehat{H},\mathcal{R}] - \delta_0^2[\hat{n},[\hat{n},\mathcal{R}]]\,, \qquad (15)$$

where $\hat{n} = \hat{n}_1 - \hat{n}_2$. We solve Eq. (15) for the adiabatic passage discussed above. Figure 9 shows fidelity (14) as the function of the noise amplitude δ_0 for three system sizes $N = 10,20,40$ where we proportionally decreased the sweeping rate ν to ensure fidelity $F \approx 1$. One striking feature of the depicted functions is a rapid decay of fidelity to $F \approx 0.5$ in the interval $0 < \delta_0 < \delta_0^*$ where $\delta_0^* = \delta_0^*(N)$. In this interval the off-diagonal elements of the density matrix $\mathcal{R}(T)$ gradually vanish. On the other hand, the diagonal elements of the density matrix remain essentially unaffected. Clearly, this result illustrates the usual quantum-to-classical transition due to a decoherence process [49–51]. Note that the larger the system is, the more it is sensitive to decoherence. Numerical results depicted in Fig. 9 indicate that δ_0^* decreases with N faster than $1/N$.

Next we briefly discuss decoherence due to particle losses. In the case of the nonconserved number of particles the master equation for the system density matrix reads

$$\frac{d\mathcal{R}}{dt} = -i[\widehat{H},\mathcal{R}] - \gamma\sum_{l=1,2}(\hat{a}_l^\dagger\hat{a}_l\mathcal{R} - 2\hat{a}_l\mathcal{R}\hat{a}_l^\dagger + \mathcal{R}\hat{a}_l^\dagger\hat{a}_l), \qquad (16)$$

where γ denotes the decay rate (see, for example, Ref. [52]). The value of γ in Eq. (16) crucially depends on the sign of interatomic interactions. For example, in the already sited experiment [34] with attractively interacting atoms the decay rate was $\gamma \approx 0.1$ which makes an impossible generation of the NOON state even for $N \sim 10$ atoms. On the other hand, it is known that a Bose-Einstein condensate of repulsively interacting atoms may have a lifetime up to a few hours that assumes $\gamma \sim 10^{-4}$ [53]. The negligible decoherence rate due to particle losses is our main reason for considering the adiabatic passage for the upper energy state of repulsively interacting atoms instead of that for the ground state of attractively interacting atoms. In all other aspects there is no conceptional difference between the adiabatic passages for the ground and upper states.

VI. PREPARATION OF THE EXCITED STATE

Finally, we discuss a method to excite the system of noninteracting bosons ($g = 0$) into the highest-energy state. A way to do this is to drive the system by periodically changing parameter δ as $\delta(t) = \delta_0 \sin(\omega t)$ where frequency ω coincides with the transition frequency between the symmetric and the antisymmetric single-particle states uniquely determined

by the parameter J. If $\delta_0 \ll J$ (the latter condition justifies the rotating-wave approximation) the problem can be solved analytically and leads to the Rabi oscillations, see Fig. 10(a). Thus, to excite the system in the upper state, we need to drive it for one-half of the Rabi period.

Another, perhaps even simpler, way to obtain the excited state (4) is to quench the system into the parameter region $\delta \gg J$ by suddenly tilting the double well. Then the time evolution of the expansion coefficients is approximately given by $c_n^{(j)}(t) = \exp(i2\,\delta n\, t) c_n^{(j)}(0)$, and after one-half of the period $T_B = \pi/\delta$ (which can be interpreted as the Bloch period) state (3) transforms into state (4), see Fig. 10(b).

VII. CONCLUSIONS

We suggested a method for creating the NOON state of Bose atoms, i.e., coherent superposition of two states in which all particles are in the same well of the double-well potential. Unlike in previous studies, which almost exclusively focused on the case of attractive interactions [54], we considered the repulsively interacting atoms that avoid the problem of particle losses. The scheme protocol consists of two steps. First, by setting the interatomic interactions to zero we transfer the system from the ground state to the upper excited state. Second, adiabatically increasing the interaction strength and simultaneously decreasing the hopping rate we transform this excited state to the NOON state. In the Fock space the latter stage can be viewed as splitting of the initially localized wave packet into two packets [55]. This process was shown to have a pseudoclassical counterpart and some quantum results, for example, the population imbalance G can be obtained by using pure classical arguments. Of course, the classical approach cannot address phase coherence between the packets, which is characterized by the fidelity F.

Formally, the suggested scheme allows us to create an arbitrary large cat state. However, any experimental realization of the scheme protocol imposes a fundamental limitation on the number of atoms due to decoherence processes present in a laboratory experiment. Here, we analyzed the decoherence caused by fluctuation of the parameter δ (the energy mismatch between the left and the right wells of the double-well potential) that appears to be crucial for the system dynamics. It was shown that there is a critical value for the fluctuation amplitude $\delta_0^* \sim 1/N$ above which the final state of the system becomes a "classical NOON state," i.e., incoherent superposition of two states in which all particles are in the same well of the double-well potential. Thus to get the NOON state with a large number of atoms every effort to reduce the fluctuation of δ should be taken.

ACKNOWLEDGMENTS

The authors acknowledge financial support from the Russian Foundation for Basic Research, Government of Krasnoyarsk Territory and the Krasnoyarsk Region Science and Technology Support Fund through Grant No. 16-42-240746.

[1] D. J. Wineland, Nobel Lecture: Superposition, entanglement, and raising Schrödinger's cat, Rev. Mod. Phys. **85**, 1103 (2013).

[2] C. Lee, J. Huang, H. Deng, H. Dai, and J. Xu, Nonlinear quantum interferometry with Bose condensed atoms, Front. Phys. **7**, 109 (2012).

[3] L. Pezzè, A. Smerzi, M. K. Oberthaler, R. Schmied, and P. Treutlein, Quantum metrology with nonclassical states of atomic ensembles, arXiv:1609.01609.

[4] C. Monroe, D. M. Meekhof, B. E. King, and D. J. Wineland, A Schrödinger cat superposition state of an atom, Science **272**, 1131 (1996).

[5] P. C. Haljan, P. J. Lee, K. A. Brickman, M. Acton, L. Deslauriers, and C. Monroe, Entanglement of trapped-ion clock states, Phys. Rev. A **72**, 062316 (2005).

[6] M. J. McDonnell, J. P. Home, D. M. Lucas, G. Imreh, B. C. Keitch, D. J. Szwer, N. R. Thomas, S. C. Webster, D. N. Stacey, and A. M. Steane, Long-Lived Mesoscopic Entanglement Outside the Lamb-Dicke Regime, Phys. Rev. Lett. **98**, 063603 (2007).

[7] H.-Y. Lo, D. Kienzler, L. de Clercq, M. Marinelli, V. Negnevitsky, B. C. Keitch, and J. P. Home, Spin-motion entanglement and state diagnosis with squeezed oscillator wavepackets, Nature (London) **521**, 336 (2015).

[8] U. R. Fischer and M.-K. Kang, Photonic Cat States from Strongly Interacting Matter Waves, Phys. Rev. Lett. **115**, 260404 (2015).

[9] D. Kienzler, C. Flühmann, V. Negnevitsky, H.-Y. Lo, M. Marinelli, D. Nadlinger, and J. P. Home, Observation of Quantum Interference Between Separated Mechanical Oscillator Wave Packets, Phys. Rev. Lett. **116**, 140402 (2016).

[10] W.-W. Zhang, S. K. Goyal, F. Gao, B. C. Sanders, and C. Simon, Creating cat states in one-dimensional quantum walks using delocalized initial states, New J. Phys. **18**, 093025 (2016).

[11] A. Smerzi, S. Fantoni, S. Giovanazzi, and S. R. Shenoy, Quantum Coherent Atomic Tunneling Between Two Trapped Bose-Einstein Condensates, Phys. Rev. Lett. **79**, 4950 (1997).

[12] J. I. Cirac, M. Lewenstein, K. Mølmer, and P. Zoller, Quantum superposition states of Bose-Einstein condensates, Phys. Rev. A **57**, 1208 (1998).

[13] R. W. Spekkens and J. E. Sipe, Spatial fragmentation of a Bose-Einstein condensate in a double-well potential, Phys. Rev. A **59**, 3868 (1999).

[14] J. Javanainen and M. Y. Ivanov, Splitting a trap containing a Bose-Einstein condensate: Atom number fluctuations, Phys. Rev. A **60**, 2351 (1999).

[15] C. Menotti, J. R. Anglin, J. I. Cirac, and P. Zoller, Dynamic splitting of a Bose-Einstein condensate, Phys. Rev. A **63**, 023601 (2001).

[16] A. P. Hines, R. H. McKenzie, and G. J. Milburn, Entanglement of two-mode Bose-Einstein condensates, Phys. Rev. A **67**, 013609 (2003).

[17] T.-L. Ho and C. Ciobanu, The Schrödinger cat family in attractive Bose gases, J. Low Temp. Phys. **135**, 257 (2004).

[18] M. Albiez, R. Gati, J. Fölling, S. Hunsmann, M. Cristiani, and M. K. Oberthaler, Direct Observation of Tunneling and

Nonlinear Self-Trapping in a Single Bosonic Josephson Junction, Phys. Rev. Lett. **95**, 010402 (2005).
[19] L. Pezzé, L. A. Collins, A. Smerzi, G. P. Berman, and A. R. Bishop, Sub-shot-noise phase sensitivity with a Bose-Einstein condensate Mach-Zehnder interferometer, Phys. Rev. A **72**, 043612 (2005).
[20] C. Lee, Adiabatic Mach-Zehnder Interferometry on a Quantized Bose-Josephson Junction, Phys. Rev. Lett. **97**, 150402 (2006).
[21] Y. P. Huang and M. G. Moore, Creation, detection, and decoherence of macroscopic quantum superposition states in double-well Bose-Einstein condensates, Phys. Rev. A **73**, 023606 (2006).
[22] E. J. Mueller, T.-L. Ho, M. Ueda, and G. Baym, Fragmentation of Bose-Einstein condensates, Phys. Rev. A **74**, 033612 (2006).
[23] R. Gati and M. K. Oberthaler, A bosonic Josephson junction, J. Phys. B: At., Mol. Opt. Phys. **40**, R61 (2007).
[24] A. I. Streltsov, O. E. Alon, and L. S. Cederbaum, Role of Excited States in the Splitting of a Trapped Interacting Bose-Einstein Condensate by a Time-Dependent Barrier, Phys. Rev. Lett. **99**, 030402 (2007).
[25] N. Teichmann and C. Weiss, Coherently controlled entanglement generation in a binary Bose-Einstein condensate, Europhys. Lett. **78**, 10009 (2007).
[26] J. Esteve, C. Gross, A. Weller, S. Giovanazzi, and M. K. Oberthaler, Squeezing and entanglement in a Bose-Einstein condensate, Nature (London) **455**, 1216 (2008).
[27] Y. Khodorkovsky, G. Kurizki, and A. Vardi, Decoherence and entanglement in a bosonic Josephson junction: Bose-enhanced quantum Zeno control of phase diffusion, Phys. Rev. A **80**, 023609 (2009).
[28] T. J. Haigh, A. J. Ferris, and M. K. Olsen, Demonstrating mesoscopic superpositions in double-well Bose-Einstein condensates, Opt. Commun. **283**, 3540 (2010).
[29] G. Mazzarella, L. Salasnich, A. Parola, and F. Toigo, Coherence and entanglement in the ground state of a bosonic Josephson junction: From macroscopic Schrödinger cat states to separable Fock states, Phys. Rev. A **83**, 053607 (2011).
[30] M. A. Garcia-March, D. R. Dounas-Frazer, and L. D. Carr, Macroscopic superposition states of ultracold bosons in a double-well potential, Front. Phys. **7**, 131 (2012).
[31] L. Dell'Anna, Analytical approach to the two-site Bose-Hubbard model: From Fock states to Schrödinger cat states and entanglement entropy, Phys. Rev. A **85**, 053608 (2012).
[32] J. Javanainen and H. Chen, Ground state of the double-well condensate for quantum metrology, Phys. Rev. A **89**, 033613 (2014).
[33] T. J. Volkoff, Optimal and near-optimal probe states for quantum metrology of number-conserving two-mode bosonic Hamiltonians, Phys. Rev. A **94**, 042327 (2016).
[34] A. Trenkwalder, G. Spagnolli, G. Semeghini, S. Coop, M. Landini, P. Castilho, L. Pezzé, G. Modugno, M. Inguscio, A. Smerzi, and M. Fattori, Quantum phase transitions with parity-symmetry breaking and hysteresis, Nat. Phys. **12**, 826 (2016).
[35] G. Spagnolli, G. Semeghini, L. Masi, G. Ferioli, A. Trenkwalder, S. Coop, M. Landini, L. Pezzé, G. Modugno, M. Inguscio, A. Smerzi, and M. Fattori, Crossing Over from Attractive to Repulsive Interactions in a Tunneling Bosonic Josephson Junction, Phys. Rev. Lett. **118**, 230403 (2017).
[36] M. Bilardello, A. Trombettoni, and A. Bassi, Collapse in ultracold Bose Josephson junctions, Phys. Rev. A **95**, 032134 (2017).
[37] H. Lee, P. Kok, and J. P. Dowling, A quantum Rosetta stone for interferometry, J. Mod. Opt. **49**, 2325 (2002).
[38] R. J. Dodd, M. Edwards, C. J. Williams, C. W. Clark, M. J. Holland, P. A. Ruprecht, and K. Burnett, Role of attractive interactions on Bose-Einstein condensation, Phys. Rev. A **54**, 661 (1996).
[39] M. A. Caprio, P. Cejnar, and F. Iachello, Excited state quantum phase transitions in many-body systems, Ann. Phys. (NY) **323**, 1106 (2008).
[40] P. Pèrez-Fernàndez, A. Relaño, J. M. Arias, P. Cejnar, J. Dukelsky, and J. E. Garcìa-Ramos, Excited-state phase transition and onset of chaos in quantum optical models, Phys. Rev. E **83**, 046208 (2011).
[41] A. Relaño, J. Dukelsky, P. Pèrez-Fernàndez, and J. M. Arias, Quantum phase transitions of atom-molecule Bose mixtures in a double-well potential, Phys. Rev. E **90**, 042139 (2014).
[42] C. Lee, Universality and Anomalous Mean-Field Breakdown of Symmetry-Breaking Transitions in a Coupled Two-Component Bose-Einstein Condensate, Phys. Rev. Lett. **102**, 070401 (2009).
[43] K. W. Mahmud, H. Perry, and W. P. Reinhardt, Quantum phase-space picture of Bose-Einstein condensates in a double well, Phys. Rev. A **71**, 023615 (2005).
[44] S. Mossmann and C. Jung, Semiclassical approach to Bose-Einstein condensates in a triple well potential, Phys. Rev. A **74**, 033601 (2006).
[45] E. M. Graefe and H. J. Korsch, Semiclassical quantization of an N-particle Bose-Hubbard model, Phys. Rev. A **76**, 032116 (2007).
[46] T. Zibold, E. Nicklas, C. Gross, and M. K. Oberthaler, Classical Bifurcation at the Transition from Rabi to Josephson Dynamics, Phys. Rev. Lett. **105**, 204101 (2010).
[47] A. R. Kolovsky and H. J. Korsch, Adiabatic scattering of atoms by a standing laser wave, Phys. Rev. A **55**, 4433 (1997).
[48] J. H. Hannay, Accuracy loss of action invariance in adiabatic change of a one-freedom Hamiltonian, J. Phys. A **19**, L1067 (1986).
[49] A. R. Kolovsky, Condition of Correspondence Between Quantum and Classical Dynamics for a Chaotic System, Phys. Rev. Lett. **76**, 340 (1996).
[50] T. Dittrich and R. Graham, Effects of weak dissipation on the long-time behavior of the quantized standard map, Europhys. Lett. **7**, 287 (1988).
[51] W. H. Zurek, Decoherence and the transition from Quantum to Classical, Phys. Today **44**(10), 36 (1991).
[52] G. Kordas, D. Witthaut, P. Buonsante, A. Vezzani, R. Burioni, A. I. Karanikas, and S. Wimberger, The dissipative Bose-Hubbard model: Methods and examples, Eur. Phys. J. Spec. Top. **224**, 2127 (2015).
[53] E. A. Cornell and C. E. Wieman, Nobel Lecture: Bose-Einstein condensation in a dilute gas, the first 70 years and some recent experiments, Rev. Mod. Phys. **74**, 875 (2002).
[54] Here, we mention the other methods for creating the NOON state of repulsively interacting atoms based on the quench [55] or lossy dynamics [56] and the works [57–61] which explore the possibility of using the two-component BEC in a single well or trap instead of the single-component BEC in a double-well potential.
[55] A. I. Streltsov, O. E. Alon, and L. S. Cederbaum, Efficient generation and properties of mesoscopic quantum superposition states in an attractive Bose–Einstein condensate threaded by a

potential barrier, J. Phys. B: At., Mol. Opt. Phys. **42**, 091004 (2009).

[56] G. Kordas, S. Wimberger, and D. Witthaut, Dissipation-induced macroscopic entanglement in an open optical lattice, Europhys. Lett. **100**, 30007 (2012).

[57] A. Micheli, D. Jaksch, J. I. Cirac, and P. Zoller, Many-particle entanglement in two-component Bose-Einstein condensates, Phys. Rev. A **67**, 013607 (2003).

[58] L. Pezzè and A. Smerzi, Entanglement, Nonlinear Dynamics, and the Heisenberg Limit, Phys. Rev. Lett. **102**, 100401 (2009).

[59] C. Gross, T. Zibold, E. Nicklas, J. Estève, and M. K. Oberthaler, Nonlinear atom interferometer surpasses classical precision limit, Nature (London) **464**, 1165 (2012).

[60] M. F. Riedel, P. Böhi, Y. Li, T. W. Hänsch, A. Sinatra, and P. Treutlein, Atom-chip-based generation of entanglement for quantum metrology, Nature (London) **464**, 1170 (2012).

[61] H. Strobel, W. Muessel, D. Linnemann, T. Zibold, D. B. Hume, L. Pezzè, A. Smerzi, and M. K. Oberthaler, Fisher information and entanglement of non-Gaussian spin states, Science **345**, 424 (2014).